Contents lists available at ScienceDirect

Separation and Purification Technology

journal homepage: http://ees.elsevier.com

Activation of electrospun lignin-based carbon fibers and their performance as self-standing supercapacitor electrodes

Francisco José García-Mateos [a], Ramiro Ruiz-Rosas [a], Juana María Rosas [a], Emilia Morallón [b], Diego Cazorla-Amorós [b], José Rodríguez-Mirasol [a,*], Tomás Cordero [a]

[a] Universidad de Málaga, Departamento de Ingeniería Química, Andalucía Tech., Escuela de Ingenierías Industriales, Campus de Teatinos s/n, 29010 Málaga, Spain
[b] Instituto de Materiales, Universidad de Alicante, Campus de San Vicente del Raspeig s/n, 03690 San Vicente del Raspeig, Alicante, Spain

ARTICLE INFO

Keywords
Lignin
Supercapacitors
Electrospinning
Carbon fibers

ABSTRACT

The production and activation of self-standing carbon electrodes from electrospun lignin fibers was analyzed in this work. Carbon microfibers were prepared at 900 °C from air-stabilized spun cloths by direct carbonization under inert atmosphere and with diluted O_2. The modifications of the porosity and surface chemistry of the carbon fibers was also studied by adding H_3PO_4 in the lignin solution and using different oxygen partial pressures during activation. The presence of phosphoric acid not only increases the porosity development and the preparation yield, but also enhances the gravimetric capacitance of the electrodes. In addition, the activation in presence of oxygen increases the surface area and the generation of wider micropores. Microporous carbon fibers with surface areas as high as 2340 $m^2\ g^{-1}$ were obtained using this method. The direct conformation of carbon fibers into binderless electrodes allows to achieve high-power rate capability supercapacitors. Activation in presence of oxygen can enhance up to 50% the energy storage of supercapacitors without compromising the power of the device (8.4 Wh kg^{-1} and P_{max} of 47 kW kg^{-1}). However, at high activation degrees, no further gain in energy density is observed due to the excessive widening of micropores, and the loss of electrical conductivity that increases the cell resistance, limiting the power capability of the device. The optimal results in terms of energy, power and durability are achieved combining low amounts of H_3PO_4 and mild activation with O_2, confirming that electrospinning of lignin is a promising method for sustainable production of self-standing supercapacitor electrodes.

1. Introduction

The necessity to reduce greenhouse effect gases and meet a rising energy demand at the same time is one of the largest challenges for our society. Shifting to a carbon-free energy system requires the development and deploy of new energy storage systems that can manage the intermittencies and decoupling between production and demand of renewable energies [1,2]. In addition, the ever-growing portable electronic device industry requests new safer, lighter, faster, wearable and low-cost energy storage systems [3,4].

For these reasons, a strong research effort is nowadays devoted to the improvement of the performance and sustainability of electrochemical energy harvesting and storage systems. Supercapacitors are electrochemical devices that store energy during polarization through the formation of the electrical double layer in the interface between a carbon-based porous electrode and the electrolyte. Given that the main storage mechanism is based on electrostatic interactions between ions and the surface of the electrode, these devices have much longer lifetime, stability and higher power capability than secondary batteries, at the cost of a lower energy density [5]. Owing to these characteristics, they are especially well suited for servicing high power demand applications, isolated electronic systems that require minimum maintenance and grid stabilization. They can be also paired with batteries in order to handle power peaks, increasing their lifetime [6].

Although recent advances in supercapacitor technology are improving their performance and driving down their costs, further efforts need to be done in order to fasten their commercial implementation. In this sense, the porous carbon electrodes are estimated to represent up to 1/3 of the cost of the device [7]. Activated carbons (ACs) are the most used porous carbon material in supercapacitor electrodes by far. Conventional ACs are usually regarded as non-expensive and sustainable materials; however, ACs required by the supercapacitor industry need to match highly demanding specifications, i.e. large specific surface areas, high electrical conductivity, high chemical and electrochemi-

* Corresponding author.
E-mail address: mirasol@uma.es (J. Rodríguez-Mirasol)

https://doi.org/10.1016/j.seppur.2020.116724
Received 5 November 2019; Received in revised form 8 Febraury 2020; Accepted 13 Febraury 2020
Available online xxx
1383-5866/

cal stability and high packing density [8]. Increasing the surface area is one of the most common strategies for enlarging the energy density of supercapacitors. However, electrical conductivity and electrochemical stability of the active phase of the electrode (i.e. activated carbon) decreases with the development of porosity. Binderless electrodes, where the active phase is casted alone in the electrode (without the addition of binders and conductivity promoters), can overcome these drawbacks owing to their improved conductivity and stability [9,10]. Moreover, certain high-end applications require additional features, such as self-standing, flexible and stretchable conformation of the electrodes [4]. Nanostructured carbon materials such as graphene, carbon nanotubes and templated carbons are usually considered as the most promising ones for matching these specifications [11–13]. The use of activated carbon fibers is also gaining increasing attention in this field because they are perfectly suited for micro-scale, wearable and/or stretchable electronic devices [14]. Unfortunately, both nanostructured carbon materials and porous carbon fibers have important drawbacks. They have high production costs, can be difficult to handle, usually involve complex synthesis procedures and they require the use of expensive reagents with low sustainability and/or have to be processed into electrodes [15].

Electrospinning is a well-known versatile, scalable, top-down technique that allows the production of polymeric nanofibers by applying a high voltage field between a solution containing the polymer and a conductive substrate [16]. Depending on the fate of the jet emitted from the polymeric solution, nanofibers (jet solidifies during fly to the substrate, i.e. electrospinning) or nanoparticles (jet breaks up into droplets, i.e. electrospray) are obtained. Electrospray/electrospinning can overcome some of the limitations of nanostructured carbon materials, making possible their steady processing into electrodes [17–19] and interestingly, they allow the production of self-standing cloths that can be later carbonized into binderless electrodes [20,21]. Polyacrylonitrile (PAN) is the precursor of choice in most of the research works concerning the preparation of porous electrospun carbon fibers for supercapacitor applications [21]. Carbonization of PAN nanofibers renders carbonized cloths with high yields, though porosity needs to be developed via physical or chemical activation in a second treatment over the carbonized fibers [22]. In addition, the sustainability of the process is low due to the fossil fuels origin of PAN and the potential evolution of toxic products (as HCN) during carbonization. Another drawback of electrospinning arises from the choice of solvent. High toxicity or non-sustainable solvents can be required in the preparation of the starting solution, due to the low solubility of polymeric precursors and the surface tension requirements of the process, while the high boiling point of some solvents makes necessary to include heaters, fan or additional devices for increase the evaporation rate in the jet.

In this context, lignin highlights as an abundant and renewable biopolymer that is obtained in large amounts as a coproduct in the pulp and paper and bio-ethanol industries. Our research group has demonstrated that it can be transformed in high-value carbon materials as activated carbons [23], carbon molecular sieves [24], hierarchical porous carbons [25], porous monoliths [26] and electrospun carbon fibers [27] owing to its worldwide availability, low cost and high carbon and aromatic contents [28]. The use of lignin as carbon precursor enhances the sustainability of the production of porous carbon electrodes, explaining the attention raised towards this topic [29–34]. The production of electrospun carbon fibers from Alcell lignin without binders or additives was reported in 2007 [35]. These lignin fibers develop microporosity during carbonization, allowing their direct use as electrodes of supercapacitors and fuel cells [36,37]. Moreover, the electrospinning is conducted using ethanol as solvent, increasing the sustainability of the process. The long air stabilization time (lasting more than 3 days) before carbonization, which is the main drawback of this method, has been recently overcome by the addition of low amounts (10–30% wt.) of phosphoric acid to the lignin solution feed to the electrospinning device [38], speeding up to 40–50 times the preparation process. Phosphoric acid also acts as activating agent during the carbonization of these fibers, increasing the surface area of the resulting carbon fibers up to 1200 $m^2\ g^{-1}$ in a single step. In addition, the presence of phosphorus-containing complexes increases the acidity [39], the oxidation [40] and the electro-oxidation resistances [41] of the carbon materials. Generally, carbonization of phosphoric acid impregnated samples takes place under inert flow; however, the presence of diluted air can increase the porosity with low yield modifications [41,42].

In this work, we report the production of self-standing porous carbon electrodes from electrospun lignin fibers. The carbon fibers were prepared by adding H_3PO_4 to the lignin solution and using different oxygen partial pressures during carbonization in order to analyze the possible changes in porosity and surface chemistry. The obtained activated fibers were directly used as binderless electrodes in order to determine their performance in aqueous based supercapacitors.

2. Experimental

2.1. Preparation of carbon fibers

Lignin fibers were prepared by electrospinning of 50% wt. Alcell® lignin in ethanol solutions by using a co-axial spinneret configuration [27]. H_3PO_4-lignin fibers were synthesized by including 5 and 15% wt. H_3PO_4 in the lignin-ethanol solution (H_3PO_4 to lignin mass ratios of 0.1 and 0.3, respectively). Flow rates of 1 mL h^{-1} for the lignin solution (inner needle of the spinneret) and 0.1 mL h^{-1} for pure ethanol (outer needle) were used for the preparation of pure lignin fibers and H_3PO_4 lignin fibers with the lowest H_3PO_4 concentration. In the case of the electrospinning of the lignin solution with higher concentration of phosphoric acid, the flow rate was increased to 3 mL h^{-1} to achieve steady jet during electrospinning of fibers. The ethanol flow rate through the outer needle was also raised up to 0.3 mL h^{-1}. Electrical field of 0.4 kV cm^{-1} was applied between the tip of the needle and the collector in all the cases. Thermostabilization of the fibers was speeded up from 5 °C h^{-1} to 60 °C h^{-1} and the holding time at 200 °C was reduced from 60 to 1 h in the case of H_3PO_4-containing fibers. Carbonization of the air stabilized fibers was performed in a horizontal tubular furnace at 900 °C in N_2 atmosphere (flow rate: 150 cm^3 STP min^{-1}). Oxygen activation treatment was carried out using different diluted air concentrations (0.5, 3.5 and 6.5% O_2) instead of inert atmosphere during the carbonization step. The gas inlet is switched to nitrogen once the thermal treatment is finished, meaning that the cooling of the sample is performed under inert conditions. The ratio between the total flow rate and the mass of stabilized fibers was always set at 150 mL $min^{-1}\ g^{-1}$. The carbon fibers were recovered in the form of carbon cloths. Those cloths prepared in the presence of H_3PO_4 were rinsed in distilled water (1 L per gram of sample) at 60 °C for 1 h and dried at 105 °C for ensure the removal of the excess H_3PO_4 before their characterization. The yield of the carbonization treatment (y_c) was determined directly calculating the remaining mass of carbonized fibers under inert atmosphere:

$$y_c = \frac{m_f}{m_o}$$

where m_f is the final mass after the carbonization treatment and m_o is the starting mass of stabilized fibers. In case of activated carbon fibers, the burn-off (BO) was calculated as follows:

$$BO = 1 - \frac{y_{end}}{y_c}$$

where y_{end} is the yield of the activation treatment (ie ratio between the final mass of activated fibers after the oxidative treatment and

the starting mass of stabilized fibers), and y_c is the yield of the carbonization treatment. The samples were prepared in duplicate and the preparation yields reported are averaged values with deviations lower than 2%. The pure lignin activated carbon fibers were denoted as CF followed by the burn-off degree in %. Similarly, The H_3PO_4-activated carbon fibers where named as PCFL (H_3PO_4:lignin mass ratio of 0.1) and PCFH (H_3PO_4:lignin mass ratio of 0.3) followed by their respective BO values.

2.2. Characterization of activated carbon fibers

The porosity of the carbonized fibers was analyzed by measuring the N_2 adsorption–desorption isotherms at −196 °C and CO_2 adsorption isotherms at 0 °C in an ASAP2020 device (Micromeritics). Prior to the analysis the carbonized fibers were outgassed overnight at 150 °C. The apparent specific surface area was estimated from the N_2 adsorption isotherm following the BET theory, while the micropore volume was determined applying the t-method (V_{mic}^{N2}). Mesopore volume (V_{mes}) was obtained by difference between the micropore volume and the volume adsorbed at relative pressure of 0.995. Narrow micropore volume (pores with sizes <0.7 nm) was obtained from the CO_2 adsorption isotherm applying the Dubinin-Radushkevich equation (V_{mic}^{CO2}) [43]. The pore size distribution (PSDs) was derived from the N_2 adsorption isotherms following the 2D-NLDFT Heterogeneous surface model [44], as applied by the Solution of Adsorption Integral Equation Using Splines (SAIEUS, http://www.nldft.com/) Software.

The chemical composition of the activated carbon fibers was analyzed using X-ray photoelectron spectroscopy (XPS) in a 5700C model Physical Electronics apparatus applying Mg Kα radiation (1253.6 eV). For an accurate identification of the oxidation state of P species, the whole XPS spectra were shifted by setting the maximum of the C1s peak position at 284.5 eV. The oxygen complexes on the surface of the activated carbon fibers were characterized by Temperature Programmed Desorption (TPD). In a typical experiment, around 10 mg of sample was heated in a TGA-DSC instrument (TA Instruments, SDT Q600 Simultaneous) from 120 °C up to 930 °C (heating rate of 20 °C min^{-1}) under inert atmosphere (Helium flow rate of 100 mL min^{-1} STP). The oxygen complexes evolve as CO and/or CO_2 during the thermal run, and the presence and amount of these gases were tracked using a mass spectrometer (Thermostar, Balzers, BSC 200) coupled at the outlet of the TGA instrument.

2.3. Electrochemical characterization of activated carbon fibers

The electrochemical characterization of the samples in 1 M H_2SO_4 solution was carried out using a standard three-electrode cell configuration in a T-type Swagelok cell equipped with titanium rods as collectors (surface of ~ 0.2 cm^2). An Ag/AgCl (3 M KCl) reference electrode was inserted in the upper connector of the cell. Round slices of the carbon cloths were cut, dried at 105 °C, weighted and directly utilized (ie as self-standing electrodes) as working and counter electrodes. Single electrode loadings of 5–8 mg cm^{-2} were used, as recommended for determination of meaningful supercapacitor parameters [45]. The thickness of the electrodes was measured in order to calculate their density. A round piece of a nylon membrane (Merck Milipore ®, pore size: 0.45 μm) was used as separator. The electrodes and membrane were soaked in the electrolyte overnight before the assemble of the cell. The electrochemical behavior of the samples was analyzed by cyclic voltammetry (CV) at a scan rate of 10 mV s^{-1} in different potential windows, in a Biologic VSP potentiostat, in order to explore the specific capacitance as positive and negative electrodes of supercapacitors as well as the potential stability window of the samples. Symmetric supercapacitors (SCs) of the activated carbon fibers were constructed using two-electrode Swagelok cells following the same procedure. The specific capacitance of the cell, the coulombic and energy efficiencies, energy and power densities were determined from a series of galvanostatic charge-discharge cycles performed at different current densities from 0.5 to 32 A g^{-1}. Maximum power density was determined by considering ideal capacitive behavior of the supercapacitor cell: $P_{MAX} = \frac{U^2}{4\hat{A}\cdot R_{cell}\hat{A}\cdot w_{electrodes}}$, where U stands for the operating voltage of the cell, R_{cell} represents the electrical cell resistance as determined from the ohmic drop on the GCD, and $w_{electrodes}$ accounts for the total weight of the dried electrodes. The cells were charged up to 1.3 V in these GCD experiments. In addition, durability tests consisting in 5000 GCD cycles at 1 A g^{-1} were performed for the activated carbon fibers with the most promising performance. As for the determination of the SC parameters, specific capacitance values of each cell were estimated from the charge delivered during the discharge branch of the GCD cycle and referred to the total weight of both electrodes. For the determination of the Ragone plot, the energy density was assessed from the area below the voltage (U) vs. discharge curve (Q) at different specific currents, whereas the power density was calculated as the ratio between the energy density and the discharge time. Finally, the coulombic and energy efficiencies were determined as the ratio between the discharge and charge time, t_d/t_c, and the discharge and charge energy, E_d/E_c. The electrochemical characterization and supercapacitors test were carried out three times for the carbon electrodes showing the best performance for each series (CF-44, PCFL-33 and PCFH-35). Standard deviations of the determined energy density at specific current of 2 A g^{-1} are lower than 5% of the averaged value.

3. Results & discussion

3.1. Preparation yields and morphology of activated carbon fibers

The sustainable production of activated carbon fibers not only requires the use of renewable sources like lignin, but also reducing preparation costs, increasing the yields and decreasing the preparation times. In this sense, the production of fibers from commercial lignin required, traditionally, the use of copolymers or the use of extensive thermal and chemical treatments [16,30,46,47]. Interestingly, Alcell lignin can be directly spun as fibers using a coaxial electrospinning device, as that used in this work. Alcell lignin has a relatively low molecular weight, so that high concentration of the biopolymer is required to achieve a viscosity of the lignin-ethanol solution high enough to enable the electrospinning process [35]. When the electrical field is applied in single electrospinning device, early clogging of the needle is produced owing to the fast evaporation of ethanol from the drop of solution that emits the jet (namely the Taylor cone). As reported in previous studies, the use of a coaxial spinneret allows to avoid the solidification of the lignin solution by providing additional ethanol that stabilizes the Taylor cone and allows steady production of fibers [35].

Once the electrospun lignin fibers are recovered as non-woven mats from the electrospinning device, they are submitted to the air stabilization step. This step is mandatory for avoiding the melting of the fibers during the carbonization step [48]. Unfortunately, thermostabilization stage is a time-demanding step, taking between 70 and 90 h in the case of pure electrospinning fibers. The addition of phosphoric acid to the lignin solution generates phosphate and polyphosphate esters that cross-links the structure of lignin fibers, bringing down the stabilization time to only 2 h [38]. This approach has been applied in this work, where H_3PO_4 to lignin mass ratios of 0.1 and 0.3 were used. Table 1 collects data regarding stabilization times and preparation yields. As can be seen, fibers casted with 0.1 and 0.3 H_3PO_4 mass ratios are stabilized in only 3 h, while pure lignin fibers require, approximately, 90 h, Table 1.

In addition, the yield of the stabilization of fibers is increased, since phosphoric acid is known to favor the polymer dehydration from very low temperatures, leading to a more condensed polyaromatic struc-

Table 1
Preparation of activated carbon fibers.

Sample	H_3PO_4:lignin mass ratio	Air Stabilization		Activation		Carbonization/ Activation yield	Overall yield
		Time	Yield	O_2 (%)	BO (%)	(%)	(%)
CF-0	0	90 h	76	0	0	37	28
CF-6				0.5	6	35	26
CF-44				3.5	44	21	16
CF-72				6.5	72	10	8
PCFL-0	0.1	3 h	86	0	0	47	40
PCFL-7				0.5	7	43	37
PCFL-33				3.5	33	31	27
PCFL-60				6.5	60	19	16
PCFH-0	0.3	3 h	87	0	0	38	33
PCFH-7				0.5	7	34	30
PCFH-35				3.5	35	25	22
PCFH-59				6.5	59	16	14

ture and therefore increasing the carbon content [48,49]. It is also observed that the use of H_3PO_4 amounts higher than 0.1 g per gram of lignin is unnecessary from the point of view of increasing the stabilization yield or time. The carbonization of these stabilized lignin fibers, at 900 °C, under inert atmosphere, produces high yields, Table 1, being comparable to those achieved using PAN as raw material [50].Oxygen activation is not usually used due to its high reactivity and difficult to control. However, the use of diluted air compared to other activating molecules, along with an adequate selection of the activation temperature can ensure a kinetic control instead of a diffusion control of the gasification reaction, providing carbon materials with a high reproducibility and reducing the energy consumption and the preparation costs. In addition, the presence of phosphoric acid during the preparation step also increases the oxidation resistance of the fibers through the formation of stable P-complexes on their surface [40], which allows a homogeneous gasification of the carbon fibers.

The effect of the oxygen presence in the preparation yield of activated fibers during carbonization was also analyzed in Table 1. As expected, additional mass loss is observed when the atmosphere for the thermal treatment is changed to diluted air. BO values between 6 and 72% are obtained as the oxygen partial pressures increases from 0.5 to 6.5%. Differently, the lesser reactivity of the H_3PO_4 containing stabilized lignin fibers delivers lower BO values and an increase in the preparation yields, see samples prepared at medium and high O_2 partial pressures in Table 1. Thus, adding H_3PO_4 in the electrospinning solution seems to be beneficial for both the stabilization and preparation yields, and for decreasing the stabilization time of the fibers.

Scanning electron microscopy was used to analyze the morphology of the carbon fibers. SEM images shown in Fig. 1 correspond to the samples obtained at the highest oxygen partial pressure. It is observed that the carbonized cloths are composed by stacks of randomly oriented fibers, showing sizes between 1 and 4 μm. The P-containing samples, PCFL-60 and PCFH-59, seem to present larger contents of bended and partially melted fibers, owing to the fast stabilization treatment utilized in their preparation. Images on the right side of Fig. 1 show that all these carbon fibers have smooth surfaces (no presence of cracks, defects and/or macropores), meaning that the air activation has been produced in a controlled way. As for the texture of the carbonized cloths, it must be noted that the cloths from the CF and PCFL series are smooth and flat, while those from the PCFH presents a cotton-like structure. In addition, the cloths become brittle when bended in the case of the samples obtained at highest BO. This is especially pronounced in the case of PCFH-59, which tends to break into pieces when is handled to construct the supercapacitor cells reported in the last section of this work.

3.2. Porosity of activated carbon fibers

The porosity parameters of all the carbon fibers prepared in this work are compiled in Table 2, while Fig. 2 presents their N_2 adsorption-desorption isotherms. All the activated carbon fibers are eminently microporous, showing type I isotherms. The addition of phosphoric acid increases the surface area and the micropore volume of the fibers obtained by carbonization in absence of oxygen (CF-0, PCFL-0, PCFH-0), increasing the apparent surface area from 840 for CF-0 to 1140 $m^2\ g^{-1}$ for PCFH-0, Table 2. These carbon fibers show mesopore volumes lower than 0.02 $cm^3\ g^{-1}$. The analysis of the mean micropore size by the calculation of $V_{mic}{}^{N2}/V_{mic}{}^{CO2}$ ratio can be an useful tool for electrochemical applications [43]. CO_2 adsorption at 0 °C only fills the narrow micropores (sizes around 0.7 nm), needing high pressures to fill the whole micropore volume (pore sizes below 2 nm). N_2 at − 196 °C can fill the total micropore volume, except the narrowest micropores (pores < 0.4 nm) [43]. Thus, the $V_{mic}{}^{N2}/V_{mic}{}^{CO2}$ ratio of CF-0 (0.87) points out the predominance of narrow micropores, while average pore size of 0.7 nm is expected for PCFL-0 given the similarities between $V_{mic}{}^{N2}$ and $V_{mic}{}^{CO2}$. Finally, $V_{mic}{}^{N2}/V_{mic}{}^{CO2}$ value of PCFH-0 (1.32) is indicative of a well-developed porosity with the presence of supermicropores (pore size between 0.7 and 2 nm).

The activation in diluted air produces the development of new pores as BO increases, as it shows the rise of the N_2 uptake at low relative pressures in the adsorption isotherms, Fig. 2. In addition, the knee of the isotherm at low relative pressures gets more rounded with the increase of BO, pointing out the widening of micropores size. In this sense, higher A_{BET} and $V_{mic}{}^{N2}$ values are delivered with the increase

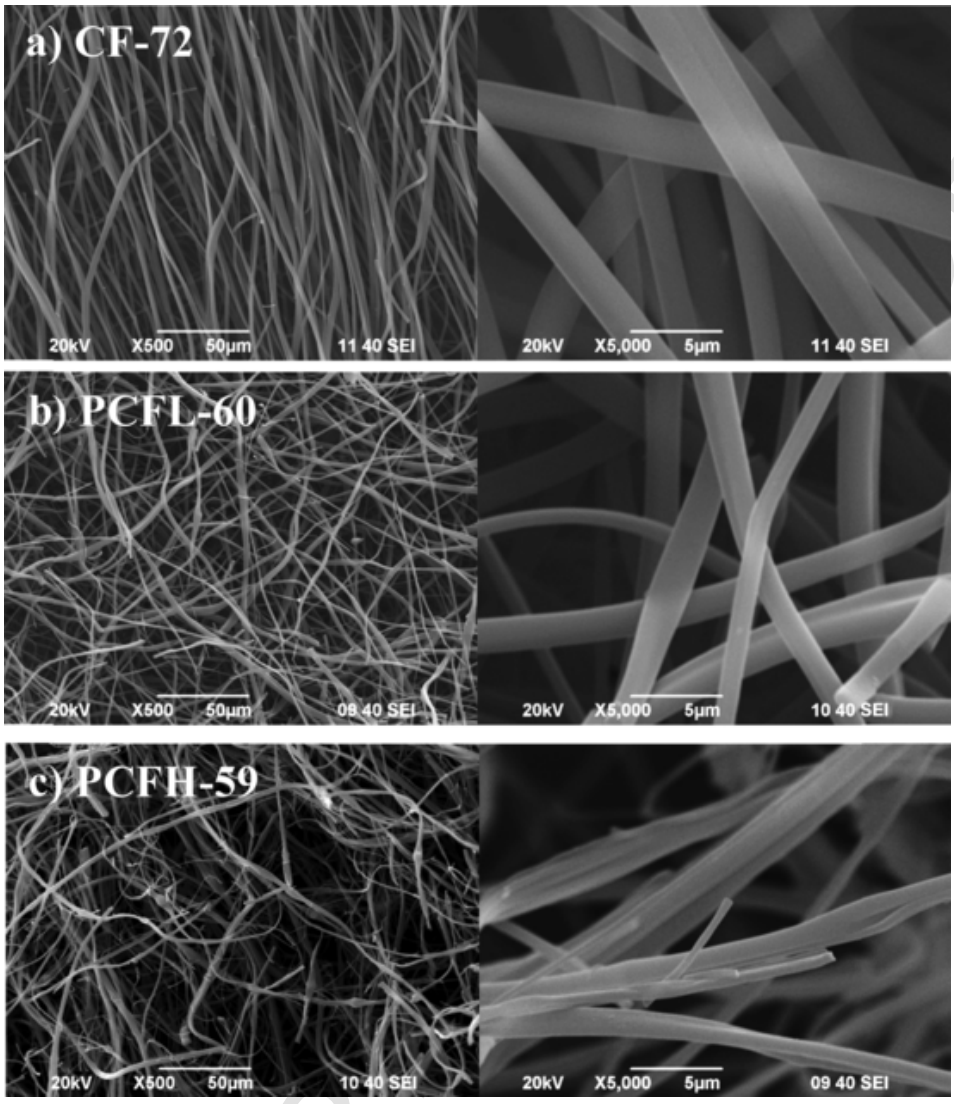

Fig. 1. SEM images of activated carbon fibers obtained using oxygen pressures of 6.5%.

Table 2
Porosity parameters of the activated carbon fibers.

Sample	A_{BET} $m^2\ g^{-1}$	V_{mes} $cm^3\ g^{-1}$	V_{mic}^{N2} $cm^3\ g^{-1}$	V_{mic}^{CO2} $cm^3\ g^{-1}$
CF-0	840	0.01	0.33	0.38
CF-6	1020	0.01	0.39	0.34
CF-44	1390	0.02	0.54	0.38
CF-72	1760	0.04	0.70	0.38
PCFL-0	950	0.01	0.36	0.36
PCFL-7	990	0.01	0.37	0.34
PCFL-33	1390	0.02	0.54	0.38
PCFL-60	1690	0.04	0.68	0.38
PCFH-0	1140	0.02	0.45	0.34
PCFH-7	1330	0.02	0.51	0.40
PCFH-35	1750	0.03	0.70	0.39
PCFH-59	2340	0.08	0.97	0.37

of BO, Table 2. Specifically, enlargements over 100% are observed for the highest BO values, as that obtained for PCFH sample from 1140 $m^2\ g^{-1}$ (BO = 0%) to 2340 $m^2\ g^{-1}$ (BO = 59%). The surface areas are higher than those obtained in the literature for electrospun lignin-based carbon fibers activated using post-treatments as KOH and CO_2 activation [16], with the advantage of combining the activation and carbonization in one step, using a green precursor and showing comparable or even higher yields.

This trend is also observed for the three series. With regard to the mean micropore size, $V_{mic}^{N2}/V_{mic}^{CO2}$ ratio increases with BO in a similar way for CF and PCFL fibers. In these series, the samples prepared using the lowest oxygen partial pressure (CF-6 and PCFL-7) show the development of micropores (higher V_{mic}^{N2} values) with a decrease in narrow micropore volume (lower V_{mic}^{CO2} values), suggesting that pore widening is the main outcome at early stages of the activation process. Moreover, at higher oxygen partial pressures, the increase in $V_{mic}^{N2}/V_{mic}^{CO2}$ values (1.4 and 1.8 for oxygen partial pressures of 3.5 and 6.5%, respectively) points out that new supermicropores are being generated, since the narrow micropore volume is barely modified. In the case of the PCFH series, the activation generates a larger widening of the microporosity, because at the same BO values than CF and PCFL, larger V_{mic}^{N2} and $V_{mic}^{N2}/V_{mic}^{CO2}$ values are obtained. Previous studies about the microporosity development during H_3PO_4 activation of lignocellulosic materials in air atmosphere reported lower porosity generation when low concentrated phosphoric acid was used [51], in agreement with these results. Still, the activation in diluted air under these conditions is highly selective towards the formation of microp-

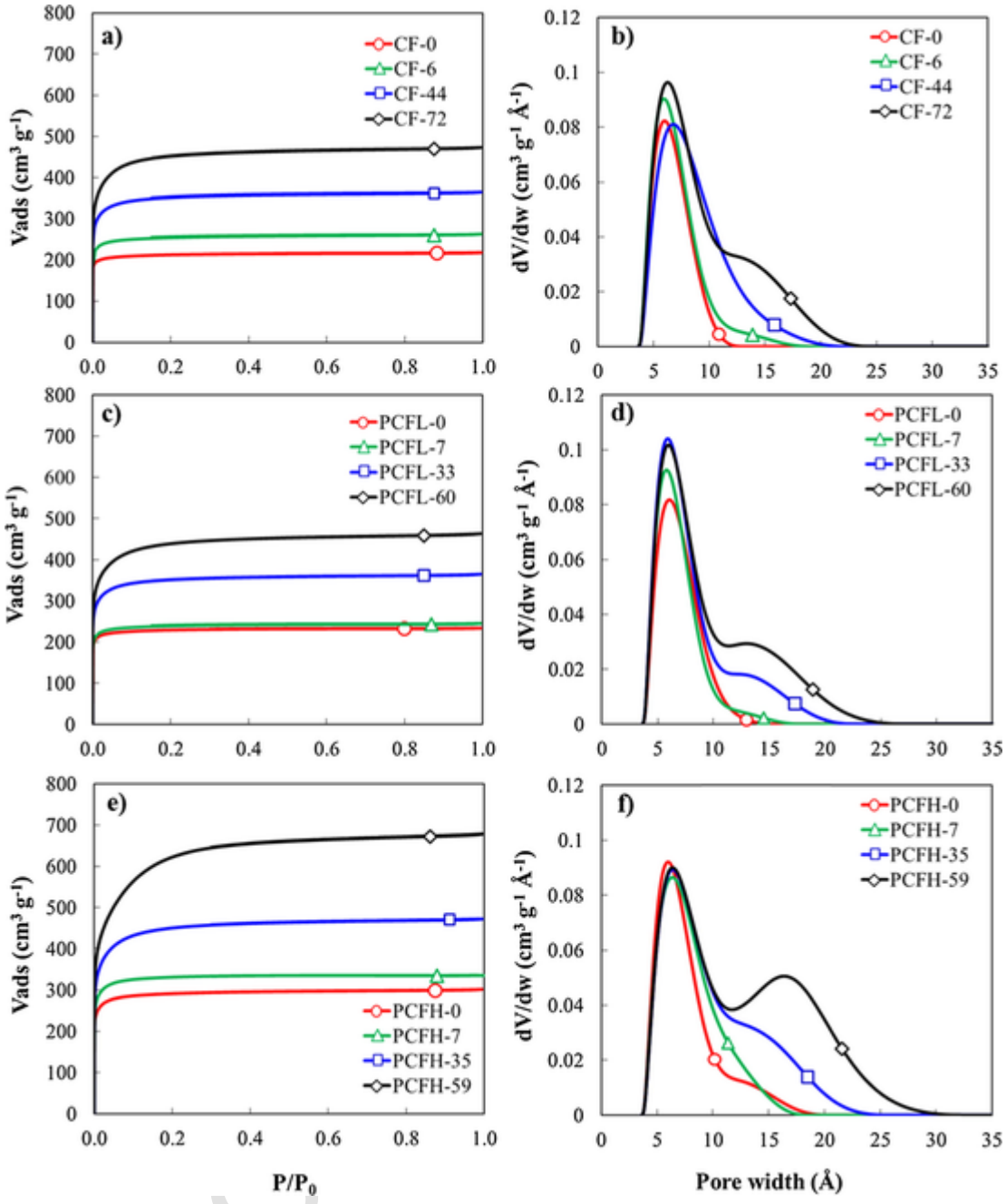

Fig. 2. N_2 adsorption-desorption isotherms at −196 °C and the derived NLDFT pore size distributions of the activated carbon fibers.

ores, with the fraction of mesopores to the total pore volume being lower than 8% for all the analyzed samples, including those of the PCFH series.

Pore size distributions derived from the N_2 adsorption isotherms are collected in Fig. 2. These PSDs clearly show the development of wider micropores as a result of the increase of the oxygen partial pressure during the carbonization of the fibers (see the appearance and rise of a new peak at ca. 15 Å in PSD of CF series, curves black, green & blue in Fig. 2**b**). The presence of low amounts of phosphoric acid does not affect this tendency, Fig. 2**d**. However, when the amount of H_3PO_4 is high enough, the new pores being developed show wider sizes (the rising peak is located at 18 Å in PCFH series, Fig. 2**f**). Previous studies about the chemical activation with H_3PO_4 of biomass waste already reported the development of mesoporosity as the amount of the activating agent increases owing to the formation of polyphosphates [49,52] . In this case, the amount of phosphoric acid is still too low to favour the formation of mesopores (which requires higher impregnation ratios [53]), only showing a widening in the micropores size range.

3.3. Surface chemistry of activated carbon fibers

P content determined by XPS analyses of the activated carbon fibers are compiled in Table 3. The study of the P 2p XPS photoemission region of these samples revealed the presence of a main peak at 134.0 eV, corresponding to the presence of C-O-P bonds from phosphate/polyphosphates groups fixed to the carbon surface [53], and at 133.2 eV related to CPO_3 and C_2PO_2 bonds [54]. The amount and oxidation state of phosphorus remains unaltered with the BO degree. The results do not provide a clear relationship between P content and

Table 3
Surface chemistry characterization of activated carbon fibers.

Sample	P_{XPS} (%wt.)	CO_{TPD} (μmol g^{-1})	$CO_{2,TPD}$ (μmol g^{-1})	O_{TPD} (%wt.)
CF-0	0	600	380	1.6
CF-6	0	1540	480	3.2
CF-44	0	2070	360	3.8
CF-72	0	2260	370	4.2
PCFL-0	2.0	2280	430	5.0
PCFL-7	1.9	2680	470	5.8
PCFL-33	1.8	2930	530	6.4
PCFL-60	1.0	3450	580	7.4
PCFH-0	1.8	1950	330	4.2
PCFH-7	1.9	2330	470	5.2
PCFH-35	1.5	2770	510	6.1
PCFH-59	1.9	3090	600	6.9

BO, suggesting that the amount of phosphorus is unrelated to the BO degree.

Fig. 3 shows the CO and CO_2 evolution profiles of the activated carbon fibers. TPD is a well-known technique that allows to identify the presence of different surface oxygen complexes attending to the differences in their thermal stability and the type of gas generated by the decomposition of the functional group. In general, the evolution of CO during TPD is related to the presence of functional groups, such as phenols, quinones, carbonyls and ethers, while CO_2 evolving groups are related to carboxylic acids, anhydrides and lactones [55,56]. However, the presence of heteroatoms can introduce changes in these classifications, as in the case of P-containing carbon materials. In them, oxidized phosphorus complexes, which have acid character, thermally decompose releasing CO at temperatures over 850 °C [57]. Thus, the CO profiles of CF series reveal the presence of quinones/carbonyls (CO evolution at 750–900 °C) as the most abundant surface oxygen groups, with a larger share of phenols (CO evolution at 650–750 °C) being found in the surface of the CF activated at medium and high burn-offs. This result is in agreement with the changes introduced in the surface chemistry of carbon materials by oxidation in air, where preferential formation of phenols is reported [58]. However, the CO TPD profile is shifted towards higher temperatures, ca. 850 °C in PCFL and PCFH samples. In them, the most abundant contribution to the CO profile seems to be that generated by the thermal reduction of C-O-P bonds [53,57]. Again, the activation of PCFL and PCFH in diluted air at medium and high BOs delivers the formation of a shoulder in the CO profile at 650 °C, which is indicative of the formation of phenol groups. A similar feature was observed when P-containing activated carbons are treated in air atmosphere at temperatures over 300 °C [57]. As for the CO_2-evolving functionalities, the CO_2 profiles indicate the presence of lactones and carboxylic acids, but their amounts are much lower than those of CO-evolving groups. The amount of carboxylic acids is higher in the P-free CF-0, while more lactones seem to be found in PCFL-0 and PCFH-0. The CO_2 profiles barely change with the BO, showing a slight rise in the ratio of lactones to carboxylic acids as the activation advances.

It is also possible to estimate the amount of surface oxygen groups by recording the concentration of the evolving gases during the TPD run. Table 3 gathers the evolved amount of CO and CO_2 for all the activated carbon fibers. It can be seen that the amount of CO_2-evolving groups is unconnected to the oxygen partial pressure used during the preparation of the activated carbon fibers (see $CO_{2,TPD}$ in Table 3). However, the amount of CO-evolving groups increases with the BO, and this behavior is also observed in all the series. When CO evolution is normalized using the A_{BET} value, the surface density of CO groups of CF series increases from 0.7 (CF-0) to 1.5 (CF-6) μmol m^{-2} when oxygen is feed during the carbonization, and it remains the same as oxygen partial pressure increases, samples CF-40 and CF-72. The surface density of CO-evolving groups for PCFL and PCFH series shows only small variations with the BO within each series, showing average values of 2.3 and 1.6 μmol m^{-2}, respectively. The surface density is higher in P-containing fibers due to the contribution of oxidized phosphorus group to the amount of evolved CO. The total amount of oxygen in the sample can be calculated combining the evolved quantities of CO and CO_2 during TPD (O_{TPD} column in Table 3).

3.4. Electrochemical characterization

The electrochemical behavior of the activated carbon fibers is studied by cyclic voltammetry measurements at low scan rate under different potential windows. First, CVs from CF, PCFL and PCH series are plotted separately in order to analyze the effect of the BO in the capacitance of the electrodes, Fig. 4. These CVs are recorded using a potential window of −0.2 to 0.8 V vs Ag/AgCl, allowing to assess the faradaic contributions from surface oxygen groups to capacitance [59,60].

The sample prepared without H_3PO_4 and under inert atmosphere, CF-0, shows a rectangular CV, characteristic of a pure capacitive behavior (Fig. 4**a**). When CF samples are prepared in presence of oxygen, an increase of the capacitance in all the potential range is observed as activation increases, including the development of broad, reversible redox peaks at potentials between 0.2 and 0.4 V vs Ag/AgCl (see CVs of CF-44 and CF-72 samples). These peaks are indicative of the occurrence of fast faradaic reactions from electroactive surface oxygen groups. The relationship between BO and electrochemical behavior is different in P-containing activated carbon fibers. In the case of PCFL series, Fig. 4**b**, there is an increase in the capacitance when the stabilized fibers are prepared in presence of oxygen (CV of PCFL-0 vs PCFL-7). However, a further increase of BO produces changes in the current of the redox peaks at 0.3 V but no shift of the peak potential is observed indicating the reversibility of the redox process. An increase of the BO in PCFH samples barely has any effect on their electrochemical behavior, Fig. 4**c**, exception made of PCFH-59, where more intense and irreversible redox peaks are observed. A direct comparison between the CVs of the most activated samples, Fig. 4**d**, reveals only minimal differences, which are accountable to the contribution of electroactive functional groups (ie the presence of irreversible redox peaks in PCFH-59).

Gravimetric capacitances are determined from the CVs shown in Fig. 4, and the obtained values are compiled in Table 4 ($\mathbf{C_g}$). The capacitance of the fibers obtained by carbonization in inert atmosphere are in agreement to previous publications [36,38], and they double the C_g values of electrodes obtained from carbonization of electrospun lignin/polyvinyl alcohol blends in 6 M KOH [61]. At first glance, the impact of BO in gravimetric capacitance is lower than expected, especially considering the observed increase in A_{BET} achieved in P-containing fibers, Table 2. In fact, the surface capacitance of these materials (C_g/A_{BET} in Table 4), although they have typical values for activated carbons [62], shows a negative trend with A_{BET}. Ideally, the gravimetric capacitance of activated carbons is expected to be proportional to the specific surface area. However, the lack of a clear relationship between capacitance and A_{BET} has been already reported in the literature [63–65]. Some authors have proposed that the wettability, the pseudocapacitance and the pore size distribution of carbon materials can have a stronger impact in capacitance than A_{BET} [15]. Wettability in aqueous electrolyte is related to the presence of polar complexes, such as surface oxygen groups [66], which increases the surface area that can be reached by the electrolyte, and pseudocapacitance in acid electrolyte is connected to the presence of CO-evolving groups [59]. Since the amount of surface oxygen groups increases with BO, Table 3, the differences in the pore size distribution seems to be the responsible

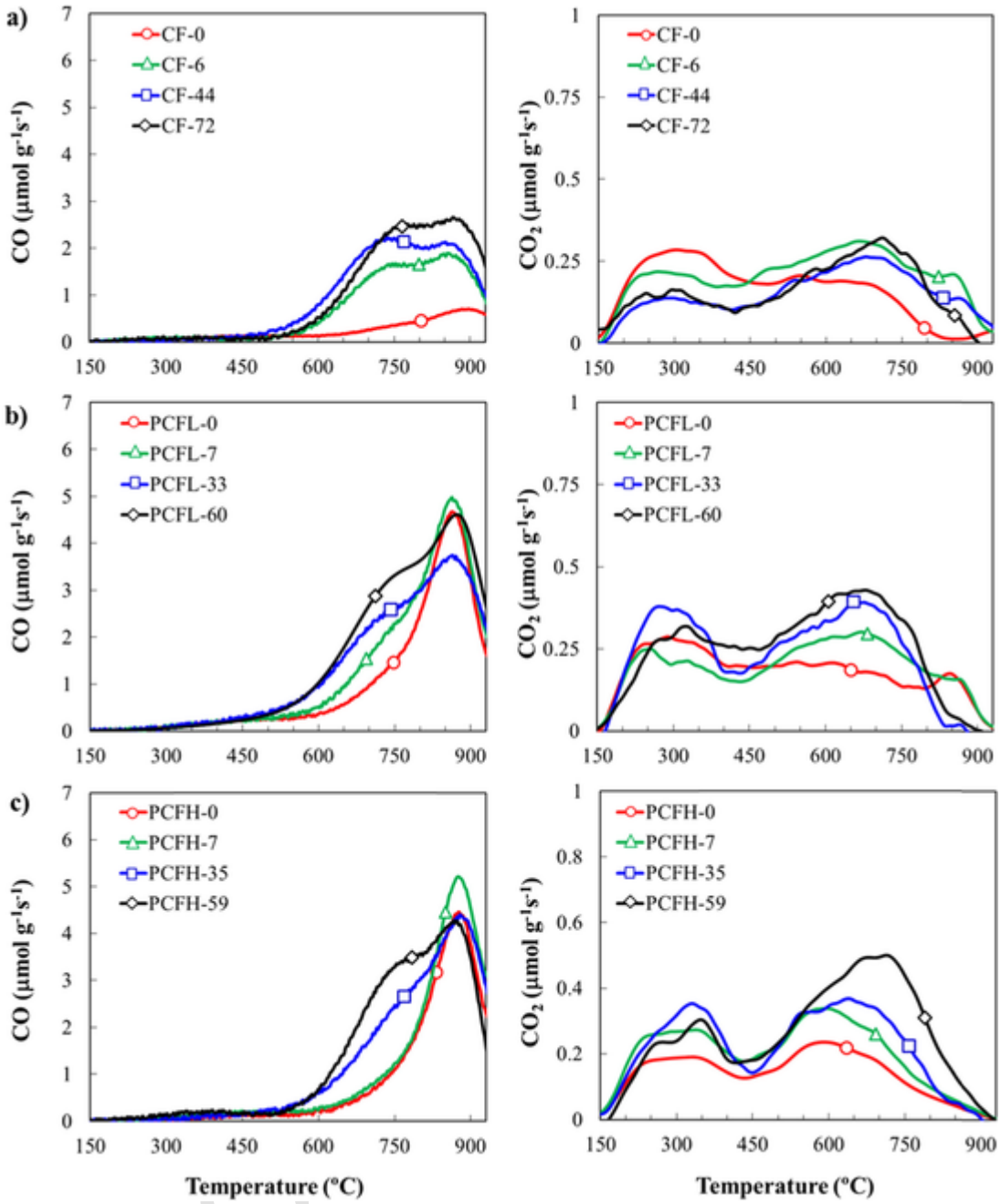

Fig. 3. CO (left side) and CO_2 (right side) TPD evolution profiles of (a) CF, (b) PCFL and (c) PCFH samples obtained at different BO.

for the decrease in surface capacitances. In this sense, several authors stated that micropores with sizes lower than the ions of the electrolyte can produce sieving effects [67], while narrow micropores matching the size of unsolvated ions increases significantly the surface capacitance [68]. On the contrary, the presence of wide micropores enlarges the distance between ions and the surface of the electrode, decreasing the surface capacitance [69]. For aqueous electrolyte, micropore sizes around 0.7–0.8 nm were proposed to maximize capacitance in aqueous electrolyte [70]. Thus, since the surface capacitance of the wide micropores developed as BO increases (see $V_{mic}{}^{N2}/V_{mic}{}^{CO2}$ ratios from Table 2 and PSDs in Fig. 2) is lower than that of narrow micropores, only minor gains in gravimetric capacitance are obtained, explaining the decrease of surface capacitance with burn-off. Volumetric capacitances have been estimated from the bulk density of the electrodes, Cv values on Table 4. In general, volumetric capacitance increases with B.O. in a lower extent than gravimetric one owing to the development of porosity, which brings down the bulk density of the electrodes. The highest Cv values are obtained for the PCFH series (98 F cm^{-3}). Volumetric capacitances do not increase with B.O. due to the loss of bulk density of the electrodes, which compensates any gaining of gravimetric capacitance. CF and PCFL show similar Cv values at comparable B.O. In these series, volumetric capacitance increases with B.O. reaching values of 80 F cm^{-3} in the case of CF-72 and 76 F cm^{-3} for PCFL-60. These values are similar to those obtained for lignin-based hierarchical porous carbons [32], although lower than the ones showed by denser binderless carbon monoliths [26,71]. Densification of electrospun carbon electrodes needs to be addressed for broadening their potential applications.

The stability potential windows of all the samples are assessed in the three-electrode cell by stepwise opening of the CV potential win-

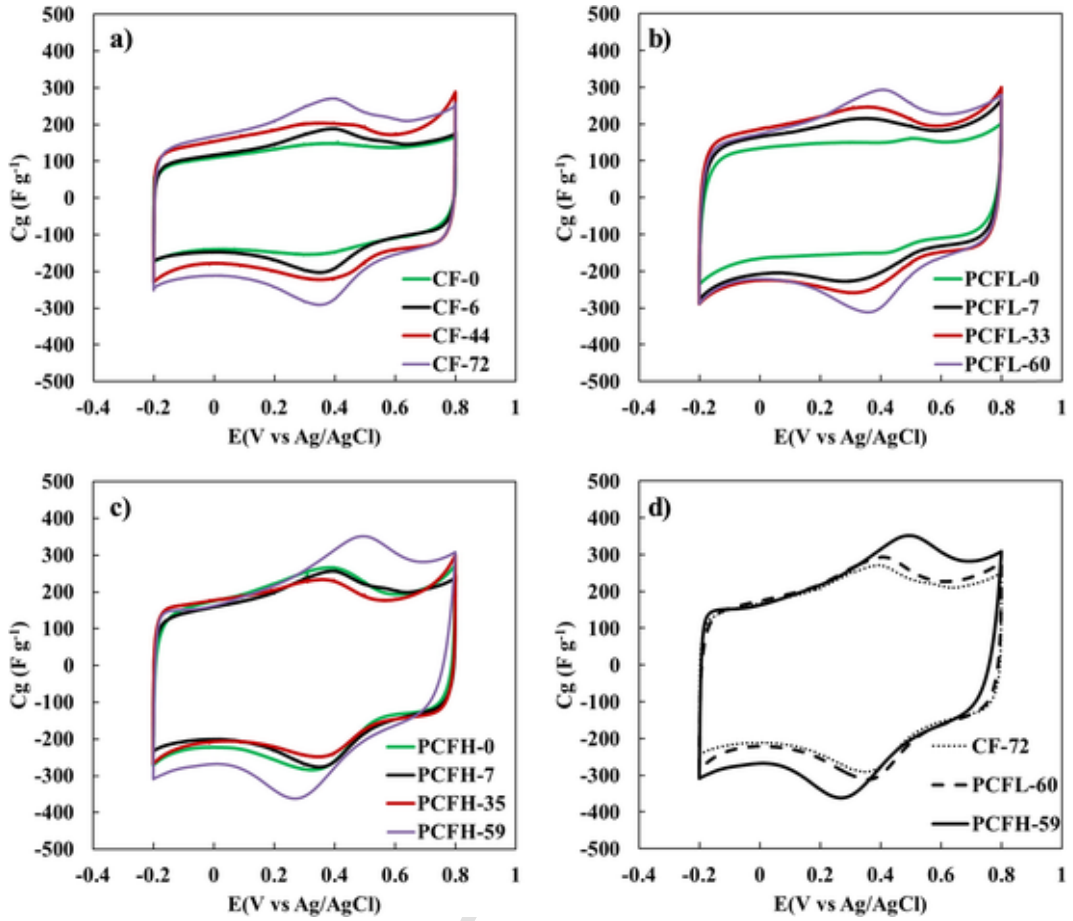

Fig. 4. Three electrode CV measurements of (a) CF, (b) PCFL and (c) PCFH samples at different BO levels. (D) Comparison between the most activated samples. Scan rate: 10 mV s^{-1}. Electrolyte: 1 M H_2SO_4.

Table 4
Three-electrode characterization of activated carbon fibers in 1 M H_2SO_4.

Sample	C_g	Bulk density	C_V	C_g/A_{BET}	OCP	$\Delta V_{max}{}^+$	$\Delta V_{max}{}^-$	$C_{g,max}{}^+$	$C_{g,max}{}^-$	U_{max}
	F g^{-1}	g cm^{-3}	F cm^{-3}	mF m^{-2}	V	V	V	F g^{-1}	F g^{-1}	V
CF-0	134	0.45	60	160	0.31	0.59	0.81	123	123	1.18
CF-6	143	0.44	62	140	0.32	0.55	0.82	181	151	1.21
CF-44	178	0.41	73	128	0.28	0.62	0.76	174	186	1.20
CF-72	206	0.39	80	117	0.35	0.55	0.83	219	194	1.17
PCFL-0	149	0.39	58	156	0.26	0.61	0.76	165	136	1.35
PCFL-7	174	0.39	67	174	0.28	0.62	0.78	200	173	1.34
PCFL-33	205	0.36	75	147	0.24	0.64	0.74	203	203	1.28
PCFL-60	218	0.35	76	129	0.23	0.63	0.73	213	196	1.31
PCFH-0	195	0.50	98	171	0.25	0.65	0.73	185	197	1.26
PCFH-7	200	0.49	98	150	0.24	0.62	0.73	189	170	1.31
PCFH-35	204	0.45	93	117	0.29	0.62	0.79	186	188	1.23
PCFH-59	240	0.41	98	102	0.28	0.63	0.78	190	200	1.23

dow. The potential limits are explored from the open circuit potential (whose values are collected in OCP column of Table 4) up to 1.0 V vs Ag/AgCl (positive potential window) and down to −0.5 V vs Ag/AgCl (negative potential window) using scan rate of 10 mV s^{-1}. The stability potential limits are stablished at the potentials where the contribution of faradaic current to the overall current is more than five percent [72]. Fig. 5 compares the voltammograms of the potential window tests for the highest BO samples of each series. The three samples can safely operate at potentials lower than −0.4 V vs Ag/AgCl. However, a large irreversible peak is developed at potentials higher than 0.9 V, which are indicative of the degradation reactions of the electrolyte and the oxidation of the electrode. The intensity of this current is slightly lower in the case of the P-containing fibers, owing to the protective effect towards electrooxidation of phosphorus groups [41]. Similar results are obtained for the rest of the samples. The available potential windows for the positive and the negative electrodes (**$\Delta V_{max}{}^+$ and $\Delta V_{max}{}^-$**, respectively), of each sample are gathered in Table 4. It is observed that the positive potential windows are narrower, and P-con-

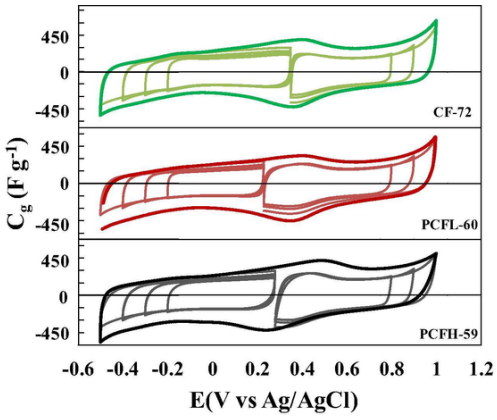

Fig. 5. CV Exploration of the stability potential windows of activated carbon fibers prepared at the highest BO. Scan rate: 10 mV s^{-1}. Electrolyte: 1 M H_2SO_4.

taining fibers usually show lower OCPs than their P-free counterparts, meaning that their negative and positive potential windows are more equilibrated. Thus, the lower OCP for P-containing fibers is an interesting observation from an application point of view.

The highest allowable voltage, U_{max}, for the symmetric supercapacitor cells (i.e. equal weight of the electrodes) are estimated from the potential window tests. Note that charge is symmetrically stored in both electrodes, $Q^+ = Q^-$, and given the dependency of charge with capacitance and voltage, the equation $C_g^+ \cdot \Delta V^+ = C_g^- \cdot \Delta V^-$ can be applied (where C_g^+ and C_g^- stands for the gravimetric capacitance of the positive and the negative electrodes as measured in the ΔV^+ and ΔV^- potential windows). $C_{g,max}^+$ and $C_{g,max}^-$ are drawn for all the samples from the CVs recorded at the maximum allowable potential window of each electrode. It has been found that the limiting charge (lower value of $C_{max,g}^{\pm} \cdot \Delta V_{max,g}^{\pm}$) is in all the cases assigned to the positive electrode. Failure of supercapacitors due to overoxidation/degradation reactions on the positive electrode in aqueous electrolytes has motivated the development of strategies based in asymmetric in mass electrodes [73] or the use of protective additives [74]. Using the limiting charge as calculated by the positive electrode and the gravimetric capacitance of the negative electrode, it is possible to estimate the maximum available voltage, $U_{max} = \Delta V_{max}^+ \cdot (1 + C_{max,g}^+ / C_{max,g}^-)$. It can be seen that most of the capacitor cells constructed using CF samples could theoretically operate at 1.2 V, while PCFL samples and PCFH-7 could reach 1.3 V (Table 4).

3.5. Characterization of the activated carbon fibers as self-standing supercapacitor electrodes

All the activated carbon fibers prepared in this work are used as self-standing electrodes for the construction of 2-electrode symmetric supercapacitor cells. These cells are constructed and characterized following the recommendations for ensuring trustable measurements of the supercapacitor performance [45,75]. In first place, the performances of the cells are analyzed using several cycles of galvanostatic charge-discharge (GCD) experiments up to 1.3 V at different specific currents ranging from 1 to 64 A g^{-1}. Fig. 6 presents the 8th cycle GCD profile at specific currents of 2 (left panel) and 16 A g^{-1} (right panel). At low specific currents, all the cells show quasi-triangular charge-discharge profiles, confirming the predominance of capacitive behavior. Gravimetric capacitances of the cells are measured from the discharge time and compiled in Table 5. In addition to the gravimetric capacitance, GCDs recorded at high specific currents are used to measure the cell resistance from the ohmic drop (i.e. drop of voltage in the charge to discharge transition), $R_{cell} = IR_{drop}/I$. Capacitances from 33 to 48 F g^{-1} are determined for these cells. At low specific currents, $Cg_{,2E}$ values seem to increase with the BO degree. However, this trend does not hold at high specific currents, where samples obtained at medium BO (CF-44, PCFL-33, PCFH-35) show the best capacitance values. This tendency can be explained by the variation in cell resistances, R_{cell} in Table 5. The samples prepared by direct carbonization have average pore sizes of 1 nm or even lower (V_{DR}^{N2}/V_{DR}^{CO2} from Table 2), increasing the diffusion resistance of ions in the porosity [8]. As the BO degree increases, micropores are widened, decreasing the diffusion resistance. However, an excess of porosity reduces the electrical conductivity of the electrode, which in turn increases the cell resistance of the samples prepared at high BO [63]. Maximum power density is estimated from the R_{cell} values considering ideal behavior of the cells and using an operating voltage of 1.3 V. Values as high as 47 kW kg^{-1} are obtained for PCFL-33, followed by 40 kW kg^{-1} shown by CF-44. These values are between the highest observed in the literature [21,36].

Energy and power densities are obtained at different specific currents. Table 5 compiles the Eg values at 2 and 16 A g^{-1}. The advantages of performing the carbonization treatment in diluted air are observed in several ways. At 2 A g^{-1} (0.65 kW kg^{-1}), the highest energy density, 8.6 Wh kg^{-1}, is obtained for CF-44, followed by PCFL-33, 8.4 Wh kg^{-1}. Note that the activation in diluted air produces energy enhancements of 50% for CF and PCFL series, while no net gain is observed for PCFH series. However, when power density is increased to 16 A g^{-1} (ca. 10 kW kg^{-1}) an increment of 41% in energy density is observed between PCFH-0 and PCFH-35, and even larger amounts are obtained in CF and PCFL series. Coulombic and energy efficiencies are also included in Table 5. As can be observed from the high columbic efficiencies, charge stored in the cell can be effectively recovered during the discharge process, and this is unaffected by the BO degree. The energy efficiency is inversely related to the ohmic drop, while curved charge-discharge profiles (i.e. deviation from the ideal triangular GCD profile) also decreases the efficiency. The highest energy efficiencies are shown by samples prepared at medium BO degrees (CF-44, PCFL-33 and PCFH-35) for a wide range of specific current values.

Ragone plots are useful for comparing the energy and power capabilities of electrochemical energy storage devices. Fig. 7 compares the Eg vs Pg profiles of all the analyzed cells. The boosted performance of samples prepared in presence of oxygen is especially notable for the PCFL series (Eg vs Pg profile of PCFL-0 is always under those for O_2-activated samples). Similar behavior is observed in the case of CF series, exception made of the highest tested power density. However, the performance of PCFH samples is barely improved with the BO degree, showing only an increase of power capability rather than energy density. The supercapacitor performance of these cells is among the highest reported in the literature for electrospun fibers, being comparable to those obtained by KOH-activated electrospun PAN nanofibers [76], and showing higher energy and slightly lower power capability than electrospun kraft lignin nanofibers activated either by CO_2 gasification or partial oxidation with an inorganic salt [29,30]. Commercial activated carbon fibers, textiles [77,78] and lignocellulosic fibers [79,80] show lower energy and power capabilities in aqueous electrolyte. Chemical activation of carbon fibers with KOH can be optimized for achieving larger specific surface area and capacitances on activated carbon fibers [81], at the cost of using additional preparation step and using non-renewable carbon precursors.

Finally, CF-72 and PCFL-33 materials are selected due to their highest performance and their 2-electrode supercapacitor cells are submitted to a durability test in order to confirm their suitability as electrodes for supercapacitor. The tests consisted in 5000 GCD cycles at 1 A g^{-1} using a cut-off voltage of 1.3 V. The capacitance retention is shown in Fig. 8. In accordance to the theoretical voltage limit established in Table 4, PCFL-33 shows a higher retention of capacitance, being able to keep around 85% of their initial capacitance. However, CF-72 shows a capacitance decay higher than 20% after 2300 cycles. The compari-

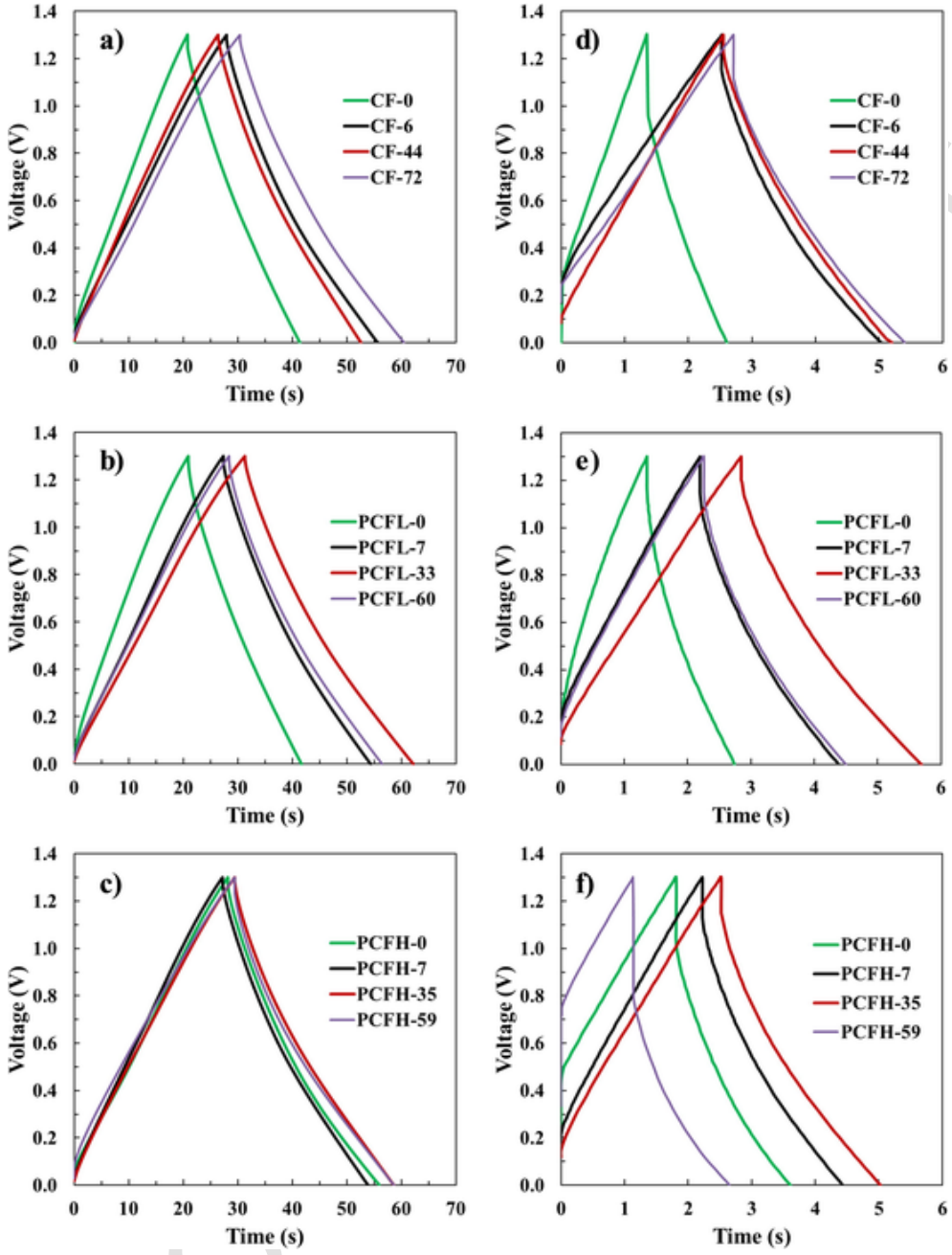

Fig. 6. 2E GCD profiles from symmetric supercapacitors loaded at 1.3 V operating at specific currents of (a–c) 2 A g^{-1} and (d–f) 16 A g^{-1}.

son between the GCDs recorded before and after the cyclability tests, Fig. 8**b**, confirms that the capacitance loss is related to the increase in the cell resistance, as depicted by the large rise in the ohmic drop. The increased electrochemical stability of P-containing activated carbon fibers electrodes is in agreement with the observations for powder P-containing porous carbons already described in the literature [41,82].

4. Conclusions

Microporous activated carbon fibers with surface areas as high as 2340 m^2 g^{-1} were successfully prepared from electrospun H_3PO_4-lignin fibers by merging phosphoric acid activation and partial gasification with oxygen during the carbonization step. The addition of phosphoric acid to lignin boosts the sustainability production of activated carbon fibers, owing to the desirable combination of higher preparation yields, shorten preparation times and higher porosity development in presence of oxygen. The activation degree can be controlled by regulating the oxygen partial pressure during the carbonization. As activation proceeds, wider micropores and electroactive functional groups are generated. The obtained activated carbon cloths showed promising performance as self-standing supercapacitor electrodes. The activation in oxygen not only enhances the energy storage up to 50% at low power density, but also improves the power capability of the electrodes. The activated carbon fibers prepared using mass H_3PO_4:lignin mass ratio of 0.1 and activated at 900 °C using 3.5% oxygen partial pressure show the best performance parameters, with energy density of 8.4 Wh kg^{-1}, maximum deliverable power of 47 kW kg^{-1} and 85% of capacitance retention after 5000 cycles at 1.3 V. Overactivation of the carbon fibers can be detrimental, producing a decrease in the maximum power density, while the use of H_3PO_4 to lignin mass ratio higher than 0.1 seems to be not useful from the point of view of the supercapacitor perfor-

Table 5
Performance parameters of the symmetric supercapacitor cells.

Sample	Specific current = 2 A g^{-1}				Specific current = 16 A g^{-1}					
	$Cg,_{2E}$ F g^{-1}	Eg Wh kg^{-1}	Eeff %	Ceff %	$Cg,_{2E}$ F g^{-1}	Eg Wh kg^{-1}	Eeff %	Ceff %	P_{max} kW kg^{-1}	R_{cell} Ω
CF-0	33	5.7	89	99	20	3.4	66	100	24.6	15.6
CF-6	47	7.9	83	99	34	4.8	69	100	24.9	15.4
CF-44	42	7.8	88	99	35	5.9	84	100	40.2	9.0
CF-72	47	8.6	86	99	37	5.7	75	100	22.5	10.6
PCFL-0	33	5.6	80	99	18	2.5	61	99	35.5	10.0
PCFL-7	42	7.5	81	99	30	4.4	68	100	31.5	11.8
PCFL-33	48	8.4	85	99	37	5.8	77	100	47.0	8.6
PCFL-60	44	7.4	85	100	30	4.3	72	100	34.4	10.4
PCFH-0	44	7.8	82	98	26	3.5	59	99	19.9	19.6
PCFH-7	42	7.0	81	98	30	4.1	65	99	29.1	14.0
PCFH-35	45	7.6	89	100	34	4.9	81	100	34.4	11.0
PCFH-59	46	7.3	81	100	16	1.4	38	100	17.0	20.6

mance. These results provide evidences that sustainable production of self-standing porous carbon electrodes with superior supercapacitor performance can be achieved by electrospinning of H_3PO_4-lignin solutions and activation in diluted air.

CRediT authorship contribution statement

Francisco José García-Mateos: Conceptualization, Investigation, Writing - original draft. **Ramiro Ruiz-Rosas:** Conceptualization, Investigation, Writing - original draft. **Juana María Rosas-Martínez:** Writing - original draft, Writing - review & editing, Visualization. **Emilia Morallón:** Supervision, Writing - review & editing. **Diego Cazorla-Amorós:** Supervision, Writing - review & editing. **José Rodríguez-Mirasol:** Project administration, Writing - review & editing, Funding acquisition. **Tomás Cordero:** Project administration, Writing - review & editing, Funding acquisition.

Declaration of Competing Interest

The authors declare that they have no known competing financial interests or personal relationships that could have appeared to influence the work reported in this paper.

Acknowledgments

We thank MICINN (RTI2018-097555-B-100 and RTI2018-095291-B-I00) for the financial support. F.J.G.M. gratefully acknowledges the assistance of MINECO through a research grant (PTA2015-11464-I).

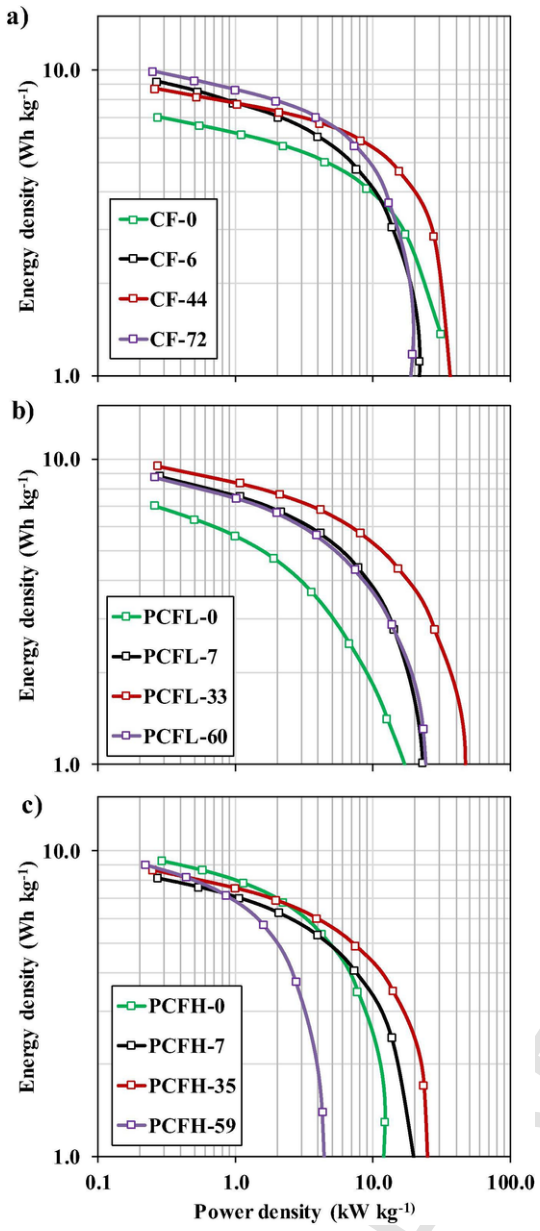

Fig. 7. Ragone plots of supercapacitor cells from the (a) CF (b) PCFL and (c) PCFH series operating at 1.3 V.

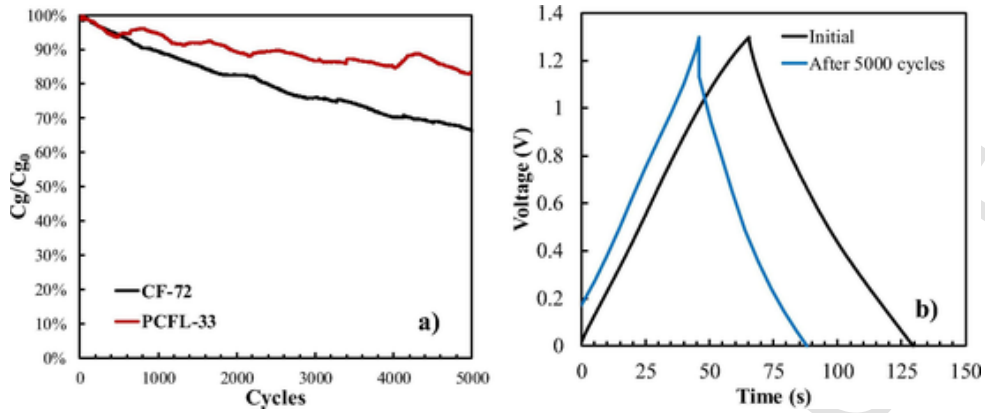

Fig. 8. (a) GCD durability test of PCFL-33 and CF-72 supercapacitor cells at cut-off voltages of 1.2 V (black lines) and 1.3 V (red line, PCFL-33) and specific current of 1 A g^{-1} (b) GCD of CF-72 cell before (black line) and after (blue line) completing the durability test. (For interpretation of the references to colour in this figure legend, the reader is referred to the web version of this article.)

References

[1] A. Hauer, C. Doetsch, M. Reuß, D. Bauer, T. Bokhoven, Energy Storage IEA Technology Collaboration Programme, Annual Report 2018, International Energy Agency, 2018. https://iea-eces.org/wp-content/uploads/public/Annual-Report-2018-Energy-Storage-TCP.pdf (accessed September 16, 2019).

[2] J.M. Carrasco, L.G. Franquelo, J.T. Bialasiewicz, E. Galvan, R.C. PortilloGuisado, M.A.M. Prats, J.I. Leon, N. Moreno-Alfonso, Power-electronic systems for the grid integration of renewable energy sources: a survey, IEEE Trans. Ind. Electron. 53 (2006) 1002–1016, doi:10.1109/TIE.2006.878356.

[3] X. Wang, X. Lu, B. Liu, D. Chen, Y. Tong, G. Shen, Flexible energy-storage devices: design consideration and recent progress, Adv. Mater. 26 (2014) 4763–4782, doi:10.1002/adma.201400910.

[4] W. Liu, M.-S. Song, B. Kong, Y. Cui, Flexible and stretchable energy storage: recent advances and future perspectives, Adv. Mater. 29 (2017) 1603436, doi:10.1002/adma.201603436.

[5] L. Guan, L. Yu, G.Z. Chen, Capacitive and non-capacitive faradaic charge storage, Electrochim. Acta 206 (2016) 464–478, doi:10.1016/j.electacta.2016.01.213.

[6] A. Yu, V. Chabot, J. Zhang, Electrochemical Supercapacitors for Energy Storage and Delivery: Fundamentals and Applications, CRC Press, 2013.

[7] M. Conte, Supercapacitors technical requirements for new applications, Fuel Cells 10 (2010) 806–818, doi:10.1002/fuce.201000087.

[8] F. Béguin, V. Presser, A. Balducci, E. Frackowiak, Carbons and electrolytes for advanced supercapacitors, Adv. Mater. 26 (2014) 2219–2251, doi:10.1002/adma.201304137.

[9] K. Nomura, H. Nishihara, N. Kobayashi, T. Asada, T. Kyotani, 4.4 V supercapacitors based on super-stable mesoporous carbon sheet made of edge-free graphene walls, Energy Environ. Sci. 12 (5) (2019) 1542–1549, doi:10.1039/C8EE03184C.

[10] S. Shiraishi, Highly-Durable Carbon Electrode for Electrochemical Capacitors, (2013). http://digital.csic.es/handle/10261/81704 (accessed September 27, 2013).

[11] C. Liu, F. Li, L.-P. Ma, H.-M. Cheng, Advanced materials for energy storage, Adv. Mater. 22 (2010) E28–E62, doi:10.1002/adma.200903328.

[12] H. Nishihara, T. Kyotani, Templated nanocarbons for energy storage, Adv. Mater. 24 (2012) 4473–4498, doi:10.1002/adma.201201715.

[13] L.L. Zhang, R. Zhou, X.S. Zhao, Graphene-based materials as supercapacitor electrodes, J. Mater. Chem. 20 (2010) 5983–5992, doi:10.1039/C000417K.

[14] D. Yu, Q. Qian, L. Wei, W. Jiang, K. Goh, J. Wei, J. Zhang, Y. Chen, Emergence of fiber supercapacitors, Chem. Soc. Rev. 44 (2015) 647–662, doi:10.1039/C4CS00286E.

[15] D. Salinas-Torres, R. Ruiz-Rosas, E. Morallón, D. Cazorla-Amorós, Strategies to enhance the performance of electrochemical capacitors based on carbon materials, Front. Mater. 6 (2019) 115, doi:10.3389/fmats.2019.00115.

[16] F.J. García-Mateos, R. Ruiz-Rosas, J.M. Rosas, J. Rodríguez-Mirasol, T. Cordero, Controlling the composition, morphology, porosity, and surface chemistry of lignin-based electrospun carbon materials, Front. Mater. 6 (2019), doi:10.3389/fmats.2019.00114.

[17] S. Martin, P.L. Garcia-Ybarra, J.L. Castillo, Electrospray deposition of catalyst layers with ultra-low Pt loadings for PEM fuel cells cathodes, J. Power Sources 195 (2010) 2443–2449, doi:10.1016/j.jpowsour.2009.11.092.

[18] H. Tang, C. Yang, Z. Lin, Q. Yang, F. Kang, C.P. Wong, Electrospray-deposition of graphene electrodes: a simple technique to build high-performance supercapacitors, Nanoscale 7 (2015) 9133–9139, doi:10.1039/C5NR00465A.

[19] J.M. Rosas, R. Ruiz-Rosas, R. Berenguer, D. Cazorla-Amorós, E. Morallón, H. Nishihara, T. Kyotani, J. Rodríguez-Mirasol, T. Cordero, Easy fabrication of superporous zeolite templated carbon electrodes by electrospraying on rigid and flexible substrates, J. Mater. Chem. A 4 (2016) 4610–4618.

[20] S. Cavaliere, S. Subianto, I. Savych, D.J. Jones, J. Rozière, Electrospinning: designed architectures for energy conversion and storage devices, Energy Environ. Sci. 4 (2011) 4761–4785, doi:10.1039/C1EE02201F.

[21] X. Lu, C. Wang, F. Favier, N. Pinna, Electrospun nanomaterials for supercapacitor electrodes: designed architectures and electrochemical performance, Adv. Energy Mater. 7 (2017) 1601301, doi:10.1002/aenm.201601301.

[22] Y.-J. Heo, H.I. Lee, J.W. Lee, M. Park, K.Y. Rhee, S.-J. Park, Optimization of the pore structure of PAN-based carbon fibers for enhanced supercapacitor performances via electrospinning, Compos. Part B: Eng. 161 (2019) 10–17, doi:10.1016/j.compositesb.2018.10.026.

[23] E. Gonzalez-Serrano, T. Cordero, J. Rodriguez-Mirasol, L. Cotoruelo, J.J. Rodriguez, Removal of water pollutants with activated carbons prepared from H 3PO4 activation of lignin from kraft black liquors, Water Res. 38 (2004) 3043–3050, doi:10.1016/j.watres.2004.04.048.

[24] J. Rodríguez-Mirasol, T. Cordero, J.J. Rodríguez, High-temperature carbons from kraft lignin, Carbon 34 (1996) 43–52, doi:10.1016/0008-6223(95)00133-6.

[25] M.J. Valero-Romero, E.M. Márquez-Franco, J. Bedia, J. Rodríguez-Mirasol, T. Cordero, Hierarchical porous carbons by liquid phase impregnation of zeolite templates with lignin solution, Micropor. Mesopor. Mater. 196 (2014) 68–78, doi:10.1016/j.micromeso.2014.04.055.

[26] P.O. Ibeh, F.J. García-Mateos, J.M. Rosas, J. Rodríguez-Mirasol, T. Cordero, Activated carbon monoliths from lignocellulosic biomass waste for electrochemical applications, J. Taiwan Inst. Chem. Eng. 97 (2019) 480–488, doi:10.1016/j.jtice.2019.02.019.

[27] R. Ruiz-Rosas, J. Bedia, M. Lallave, I.G. Loscertales, A. Barrero, J. Rodríguez-Mirasol, T. Cordero, The production of submicron diameter carbon fibers by the electrospinning of lignin, Carbon 48 (2010) 696–705, doi:10.1016/j.carbon.2009.10.014.

[28] J.M. Rosas, R. Berenguer, M.J. Valero-Romero, J. Rodríguez-Mirasol, T. Cordero, Preparation of different carbon materials by thermochemical conversion of lignin, Front. Mater. 1 (2014), doi:10.3389/fmats.2014.00029.

[29] P. Schlee, S. Herou, R. Jervis, P.R. Shearing, D.J.L. Brett, D. Baker, O. Hosseinaei, P. Tomani, M.M. Murshed, Y. Li, M.J. Mostazo-López, D. Cazorla-Amorós, A.B.J. Sobrido, M.-M. Titirici, Free-standing supercapacitors from Kraft lignin nanofibers with remarkable volumetric energy density, Chem. Sci. 10 (2019) 2980–2988, doi:10.1039/C8SC04936J.

[30] P. Schlee, O. Hosseinaei, D. Baker, A. Landmér, P. Tomani, M.J. Mostazo-López, D. Cazorla-Amorós, S. Herou, M.-M. Titirici, From waste to wealth: from Kraft Lignin to free-standing supercapacitors, Carbon 145 (2019) 470–480, doi:10.1016/j.carbon.2019.01.035.

[31] S. Hu, S. Zhang, N. Pan, Y.-L. Hsieh, High energy density supercapacitors from lignin derived submicron activated carbon fibers in aqueous electrolytes, J. Power Sources 270 (2014) 106–112, doi:10.1016/j.jpowsour.2014.07.063.

[32] R. Ruiz-Rosas, M.J. Valero-Romero, D. Salinas-Torres, J. Rodríguez-Mirasol, T. Cordero, E. Morallón, D. Cazorla-Amorós, Electrochemical performance of hierarchical porous carbon materials obtained from the infiltration of Lignin into zeolite templates, ChemSusChem 7 (2014) 1458–1467, doi:10.1002/cssc.201301408.

[33] S. Chatterjee, T. Saito, Lignin-derived advanced carbon materials, ChemSusChem 8 (2015) 3941–3958, doi:10.1002/cssc.201500692.

[34] J.L. Espinoza-Acosta, P.I. Torres-Chávez, J.L. Olmedo-Martínez, A. Vega-Rios, S. Flores-Gallardo, E.A. Zaragoza-Contreras, Lignin in storage and renewable energy applications: a review, J. Energy Chem. 27 (2018) 1422–1438, doi:10.1016/j.jechem.2018.02.015.

[35] M. Lallave, J. Bedia, R. Ruiz-Rosas, J. Rodríguez-Mirasol, T. Cordero, J.C. Otero, M. Marquez, A. Barrero, I.G. Loscertales, Filled and hollow carbon nanofibers by coaxial electrospinning of alcell lignin without binder polymers, Adv. Mater. 19 (2007) 4292–4296, doi:10.1002/adma.200700963.

[36] R. Berenguer, F.J. García-Mateos, R. Ruiz-Rosas, D. Cazorla-Amorós, E. Morallón, J. Rodríguez-Mirasol, T. Cordero, Biomass-derived binderless fibrous carbon electrodes for ultrafast energy storage, Green Chem. 18 (2016) 1506–1515.

[37] F.J. García-Mateos, T. Cordero-Lanzac, R. Berenguer, E. Morallón, D. Cazorla-Amorós, J. Rodríguez-Mirasol, T. Cordero, Lignin-derived Pt supported carbon (submicron)fiber electrocatalysts for alcohol electro-oxidation, Appl. Catal. B 211 (2017) 18–30, doi:10.1016/j.apcatb.2017.04.008.

[38] F.J. García-Mateos, R. Berenguer, M.J. Valero-Romero, J. Rodríguez-Mirasol, T. Cordero, Phosphorus functionalization for the rapid preparation of

highly nanoporous submicron-diameter carbon fibers by electrospinning of lignin solutions, J. Mater. Chem. A 6 (2018) 1219–1233, doi:10.1039/C7TA08788H.
[39] J. Bedia, J.M. Rosas, J. Márquez, J. Rodríguez-Mirasol, T. Cordero, Preparation and characterization of carbon based acid catalysts for the dehydration of 2-propanol, Carbon 47 (2009) 286–294, doi:10.1016/j.carbon.2008.10.008.
[40] J.M. Rosas, R. Ruiz-Rosas, J. Rodríguez-Mirasol, T. Cordero, Kinetic study of the oxidation resistance of phosphorus-containing activated carbons, Carbon 50 (2012) 1523–1537, doi:10.1016/j.carbon.2011.11.030.
[41] R. Berenguer, R. Ruiz-Rosas, A. Gallardo, D. Cazorla-Amorós, E. Morallón, H. Nishihara, T. Kyotani, J. Rodríguez-Mirasol, T. Cordero, Enhanced electro-oxidation resistance of carbon electrodes induced by phosphorus surface groups, Carbon 95 (2015) 681–689, doi:10.1016/j.carbon.2015.08.101.
[42] R. Ruiz-Rosas, F.J. García-Mateos, M. del C. Gutiérrez, J. Rodríguez-Mirasol, T. Cordero, About the role of porosity and surface chemistry of phosphorus-containing activated carbons in the removal of micropollutants, Front. Mater. 6 (2019). http://doi.org/10.3389/fmats.2019.00134.
[43] D. Cazorla-Amorós, J. Alcañiz-Monge, M.A. de la Casa-Lillo, A. Linares-Solano, CO2 As an adsorptive to characterize carbon molecular sieves and activated carbons, Langmuir 14 (1998) 4589–4596, doi:10.1021/la980198p.
[44] J. Jagiello, J.P. Olivier, 2D-NLDFT adsorption models for carbon slit-shaped pores with surface energetical heterogeneity and geometrical corrugation, Carbon 55 (2013) 70–80.
[45] M.D. Stoller, R.S. Ruoff, Best practice methods for determining an electrode material's performance for ultracapacitors, Energy Environ. Sci. 3 (2010) 1294–1301, doi:10.1039/C0EE00074D.
[46] M. Kumar, M. Hietala, K. Oksman, Lignin-Based Electrospun Carbon Nanofibers, Front. Mater. 6 (2019), doi:10.3389/fmats.2019.00062.
[47] J.F. Kadla, S. Kubo, R.A. Venditti, R.D. Gilbert, A.L. Compere, W. Griffith, Lignin-based carbon fibers for composite fiber applications, Carbon 40 (2002) 2913–2920, doi:10.1016/S0008-6223(02)00248-8.
[48] J.L. Braun, K.M. Holtman, J.F. Kadla, Lignin-based carbon fibers: Oxidative thermostabilization of kraft lignin, Carbon 43 (2005) 385–394, doi:10.1016/j.carbon.2004.09.027.
[49] M. Jagtoyen, F. Derbyshire, Activated carbons from yellow poplar and white oak by H3PO4 activation, Carbon 36 (1998) 1085–1097, doi:10.1016/S0008-6223(98)00082-7.
[50] Y. Yang, Z. Mei-Hua, X. Gang, J. Zheng-Xiong, Preparation and characterization of PAN-based ultra-fine activated carbon fiber adsorbent, J Porous Mater. 18 (2011) 379–387, doi:10.1007/s10934-010-9388-y.
[51] M. Molina-Sabio, F. Caturla, F. Rodriguez-Reinoso, Influence of the atmosphere used in the carbonization of phosphoric acid impregnated peach stones, Carbon 33 (1995) 1180–1182, doi:10.1016/0008-6223(95)91248-6.
[52] M. Molina-Sabio, F. RodRíguez-Reinoso, F. Caturla, M.J. Sellés, Porosity in granular carbons activated with phosphoric acid, Carbon 33 (1995) 1105–1113, doi:10.1016/0008-6223(95)00059-M.
[53] J.M. Rosas, J. Bedia, J. Rodríguez-Mirasol, T. Cordero, HEMP-derived activated carbon fibers by chemical activation with phosphoric acid, Fuel 88 (2009) 19–26, doi:10.1016/j.fuel.2008.08.004.
[54] X. Wu, L.R. Radovic, Inhibition of catalytic oxidation of carbon/carbon composites by phosphorus, Carbon 44 (2006) 141–151, doi:10.1016/j.carbon.2005.06.038.
[55] J.L. Figueiredo, M.F.R. Pereira, M.M.A. Freitas, J.J.M. Órfão, Modification of the surface chemistry of activated carbons, Carbon 37 (1999) 1379–1389, doi:10.1016/S0008-6223(98)00333-9.
[56] M.C. Román-Martínez, D. Cazorla-Amorós, A. Linares-Solano, C.S.-M. de Lecea, Tpd and TPR characterization of carbonaceous supports and Pt/C catalysts, Carbon 31 (1993) 895–902, doi:10.1016/0008-6223(93)90190-L.
[57] M.J. Valero-Romero, F.J. García-Mateos, J. Rodríguez-Mirasol, T. Cordero, Role of surface phosphorus complexes on the oxidation of porous carbons, Fuel Process. Technol. 157 (2017) 116–126, doi:10.1016/j.fuproc.2016.11.014.
[58] I.I. Salame, T.J. Bandosz, Surface chemistry of activated carbons: combining the results of temperature-programmed desorption, Boehm, and potentiometric titrations, J. Colloid Interface Sci. 240 (2001) 252–258, doi:10.1006/jcis.2001.7596.
[59] M.J. Bleda-Martínez, J.A. Maciá-Agulló, D. Lozano-Castelló, E. Morallón, D. Cazorla-Amorós, A. Linares-Solano, Role of surface chemistry on electric double layer capacitance of carbon materials, Carbon 43 (2005) 2677–2684, doi:10.1016/j.carbon.2005.05.027.
[60] M.J. Bleda-Martínez, D. Lozano-Castelló, E. Morallón, D. Cazorla-Amorós, A. Linares-Solano, Chemical and electrochemical characterization of porous carbon materials, Carbon 44 (2006) 2642–2651, doi:10.1016/j.carbon.2006.04.017.
[61] C. Lai, Z. Zhou, L. Zhang, X. Wang, Q. Zhou, Y. Zhao, Y. Wang, X.-F. Wu, Z. Zhu, H. Fong, Free-standing and mechanically flexible mats consisting of electrospun carbon nanofibers made from a natural product of alkali lignin as binder-free electrodes for high-performance supercapacitors, J. Power Sources 247 (2014) 134–141, doi:10.1016/j.jpowsour.2013.08.082.
[62] D. Qu, Studies of the activated carbons used in double-layer supercapacitors, J. Power Sources 109 (2002) 403–411, doi:10.1016/S0378-7753(02)00108-8.
[63] O. Barbieri, M. Hahn, A. Herzog, R. Kötz, Capacitance limits of high surface area activated carbons for double layer capacitors, Carbon 43 (2005) 1303–1310, doi:10.1016/j.carbon.2005.01.001.
[64] T.A. Centeno, M. Hahn, J.A. Fernández, R. Kötz, F. Stoeckli, Correlation between capacitances of porous carbons in acidic and aprotic EDLC electrolytes, Electrochem. Commun. 9 (2007) 1242–1246, doi:10.1016/j.elecom.2007.01.031.
[65] B. Lobato, L. Suárez, L. Guardia, T.A. Centeno, Capacitance and surface of carbons in supercapacitors, Carbon 122 (2017) 434–445, doi:10.1016/j.carbon.2017.06.083.
[66] B. Szubzda, A. Szmaja, A. Halama, Influence of structure and wettability of supercapacitor electrodes carbon materials on their electrochemical properties in water and organic solutions, Electrochim. Acta 86 (2012) 255–259, doi:10.1016/j.electacta.2012.08.060.
[67] G. Salitra, A. Soffer, L. Eliad, Y. Cohen, D. Aurbach, Carbon electrodes for double-layer capacitors i. relations between ion and pore dimensions, J. Electrochem. Soc. 147 (2000) 2486–2493, doi:10.1149/1.1393557.
[68] J. Chmiola, G. Yushin, Y. Gogotsi, C. Portet, P. Simon, P.L. Taberna, Anomalous increase in carbon capacitance at pore sizes less than 1 nanometer, Science 313 (2006) 1760–1763, doi:10.1126/science.1132195.
[69] C. Largeot, C. Portet, J. Chmiola, P.-L. Taberna, Y. Gogotsi, P. Simon, Relation between the ion size and pore size for an electric double-layer capacitor, J. Am. Chem. Soc. 130 (2008) 2730–2731, doi:10.1021/ja7106178.
[70] C. Vix-Guterl, E. Frackowiak, K. Jurewicz, M. Friebe, J. Parmentier, F. Béguin, Electrochemical energy storage in ordered porous carbon materials, Carbon 43 (2005) 1293–1302, doi:10.1016/j.carbon.2004.12.028.
[71] M. Kunowsky, A. Garcia-Gomez, V. Barranco, J.M. Rojo, J. Ibañez, J.D. Carruthers, A. Linares-Solano, Dense carbon monoliths for supercapacitors with outstanding volumetric capacitances, Carbon. (n.d.). http://doi.org/10.1016/j.carbon.2013.11.034.
[72] D. Weingarth, H. Noh, A. Foelske-Schmitz, A. Wokaun, R. Kötz, A reliable determination method of stability limits for electrochemical double layer capacitors, Electrochim. Acta 103 (2013) 119–124, doi:10.1016/j.electacta.2013.04.057.
[73] C. Peng, S. Zhang, X. Zhou, G.Z. Chen, Unequalisation of electrode capacitances for enhanced energy capacity in asymmetrical supercapacitors, Energy Environ. Sci. 3 (2010) 1499–1502, doi:10.1039/C0EE00228C.
[74] R. Ruiz-Rosas, I. Fuentes, C. Viñas, F. Teixidor, E. Morallón, D. Cazorla-Amorós, Tailored metallacarboranes as mediators for boosting the stability of carbon-based aqueous supercapacitors, Sustain. Energy Fuels 2 (2018) 345–352, doi:10.1039/C7SE00503B.
[75] Y. Gogotsi, P. Simon, True performance metrics in electrochemical energy storage, Science 334 (2011) 917–918, doi:10.1126/science.1213003.
[76] E.J. Ra, E. Raymundo-Piñero, Y.H. Lee, F. Béguin, High power supercapacitors using polyacrylonitrile-based carbon nanofiber paper, Carbon 47 (2009) 2984–2992, doi:10.1016/j.carbon.2009.06.051.
[77] L. Bao, X. Li, Towards textile energy storage from cotton T-shirts, Adv. Mater. 24 (2012) 3246–3252, doi:10.1002/adma.201200246.
[78] J.F. Snyder, E.L. Wong, C.W. Hubbard, Evaluation of commercially available carbon fibers, fabrics, and papers for potential use in multifunctional energy storage applications, J. Electrochem. Soc. 156 (2009) A215, doi:10.1149/1.3065070.
[79] R. Farma, M. Deraman, A. Awitdrus, I.A. Talib, E. Taer, N.H. Basri, J.G. Manjunatha, M.M. Ishak, B.N.M. Dollah, S.A. Hashmi, Preparation of highly porous binderless activated carbon electrodes from fibres of oil palm empty fruit bunches for application in supercapacitors, Bioresour. Technol. 132 (2013) 254–261, doi:10.1016/j.biortech.2013.01.044.
[80] V. Subramanian, C. Luo, A.M. Stephan, K.S. Nahm, S. Thomas, B. Wei, Supercapacitors from activated carbon derived from banana fibers, J. Phys. Chem. C. 111 (2007) 7527–7531, doi:10.1021/jp067009t.
[81] K. Babel, K. Jurewicz, KOH activated carbon fabrics as supercapacitor material, J. Phys. Chem. Solids 65 (2004) 275–280, doi:10.1016/j.jpcs.2003.08.023.
[82] C. Huang, T. Sun, D. Hulicova-Jurcakova, Wide Electrochemical Window of Supercapacitors from Coffee Bean-Derived Phosphorus-Rich Carbons, ChemSusChem 6 (2013) 2330–2339, doi:10.1002/cssc.201300457.